ACS OMEGA

http://pubs.acs.org/journal/acsodf

Article

Eco-friendly Silane-Based Coating for Mitigation of Carbon Steel Corrosion in Marine Environments

Mohammad H. BinSabt,* Fadhel A. Azeez, and Nour Suleiman

Cite This: *ACS Omega* 2023, 8, 12886−12898

Read Online

ACCESS | Metrics & More | Article Recommendations | Supporting Information

ABSTRACT: Losses from corrosion contribute roughly 3−5% of the gross domestic product of developed nations, and among the many methods used to avoid corrosion, using silane-based coatings is seen to be of the biggest importance due to their low toxicity and superior adhesive qualities. It is essential to develop an anti-corrosion coating that is efficient, economical, and eco-friendly. The corrosion resistance and durability of various silane-based coatings such as 1,2-bis(triethoxysilyl)ethane (BTSE), bis[3-(triethoxysilyl)propyl]tetrasulfide (TESPT), and vinyltrimethylsilane (VTES) for carbon steel 1018 substrates were investigated in a high-salinity environment (4.5 wt % NaCl). The corrosion resistance performance was evaluated via potentiodynamic polarization (PDP) and electrochemical impedance spectroscopy (EIS) techniques. Results revealed that the TESPT film (pH ≈ 7) has the best corrosion resistance performance on the carbon steel surface in the aggressive chloride environment, that is, 99.6%. The high corrosion resistance of the TESPT film is due to the hydrophobic nature of this silane, which leads to the formation of a stable and dense film. These results were supported by X-ray photoelectron spectroscopy (XPS), scanning electron microscopy (SEM), and energy-dispersive X-ray spectroscopy (EDX) analyses.

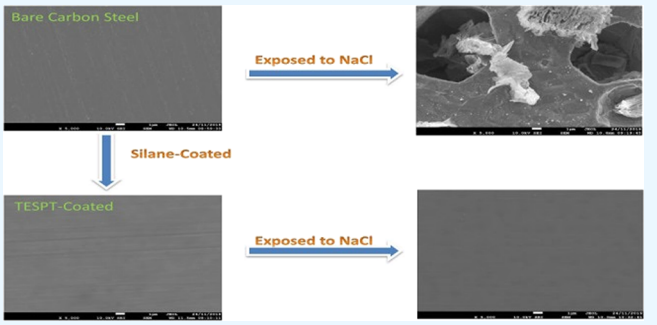

1. INTRODUCTION

One of the major problems across many industries is metal corrosion, which raises manufacturing costs and compromises safety and performance. Metal and related alloys such as mild steel, magnesium, copper, and aluminum are highly susceptible to corrosion in aggressive environments leading to considerable economic loss and safety failures.[1] Carbon steel is widely used as a raw material in the metallurgical industry where it is one of the most important raw materials. Marine environments are among the most prone to corrosion because of temperature gradients, fluctuations in flow velocity, and the presence of corrosive constituents such as inorganic salts, bio contaminants, dissolved oxygen along with other gases, and high chloride concentrations.[2−4] Consequently, if extra efforts and well-planned practices are utilized to control the corrosion process, the corrosion losses and associated economic effects could be dramatically reduced. Different methods have been employed to control the corrosion process, including material selection,[5] using corrosion inhibitors,[6] cathodic protection,[7] anodic protection,[8] and the use of protective coatings.[9] Corrosion-resistant coatings act as barriers that isolate the metal surface from the corrosive environments. This method of protecting metals against corrosion is widely used for metallic equipment in chemical plants, offshore structures, and underground structures (e.g., tanks, oil, gas pipelines, etc.).

Anti-corrosion coatings include metallic coatings, conversion coatings, glass coatings, ceramic coatings, and organic coatings. The metallic coating could be either thin nanometer-sized single-metal or multicomponent alloy layers or thicker coatings with nanoparticles of a second phase.[10] One of the most economical methods of surface modification of steel substrates is chemical conversion coatings or surface passivation. Electrochemical or chemical processes are used to turn the covered surface into a coating. The most common processes for forming conversion coatings are phosphatizing,[11] chromating,[12] and anodic oxidation.[13] The phosphate coating is resulted from immersing into or spraying the metal surface with acidic phosphate solutions. It is commonly used for zinc, steel, and aluminum. The resulting porous phosphate layer is characterized by strong adhesion to metals and good corrosion resistance. The other form of conversion coating is the chromate conversion coating, which is frequently applied on aluminum, zinc, and magnesium. This coating layer is formed from a reaction between the metal surface and an acidic chromate solution, most commonly sodium bichromate. The use of chromium-based conversion coatings is currently

Received: January 2, 2023
Accepted: March 8, 2023
Published: April 3, 2023

prohibited. On the other hand, the anodic oxidation process produces an oxide film on the metal surface by electrolysis for the purpose of increasing the corrosion resistance of the surface. These coatings involve aluminum, vanadium, zirconium, molybdenum, cerium, nickel, potassium, and zinc-rich layers.

Some metals are surrounded by highly corrosive environments that need protective coatings with thick layers to protect the metal from corrosion attacks. In such conditions, it is preferable to use glass coating,[14] cured inorganic silicates,[15] ceramic coating,[16] sulfur,[17] graphite,[18] and carbon.[19,20] Glass and ceramic coatings can handle all environments except in hydrofluoric and caustic ones. Some limitations may restrict the use of glass and ceramics where they are brittle and sensitive to thermal shock and their mechanical strength is low. Graphite and carbon have the ability to withstand rapid changes in temperature.[1]

The organic coating consists of a thin barrier that is applied on the metal to isolate its surface from aggressive environments. This type of coating involves paints, lacquers,[21] and varnishes,[22] which are frequently used for coating large areas. Meanwhile, organic polymeric coatings are the most common type of protective materials.[23,24]

Merging the properties of organic materials and inorganic ones led to novel hybrid organic−inorganic corrosion resistance coatings, which become one of the most effective techniques of surface protection.[25,26] The most widely applied hybrid inorganic−organic material is modified organosilanes (adhesion promoter).[27,28] They are a great replacement for chromate and phosphate coatings because they are non-toxic and inexpensive as well as environmentally safe. These compounds have a general formula R_nSiX_{4-n}, where R is an organic group, for example, alkyl, glycidoxypropyl, amidogen, or others, and X is a hydrolyzable group (alkoxy: −OMe or −OEt). Owing to its unique chemical structure, the organosilane film serves as a bridge between the metal and the anticorrosion coating. Their molecules demonstrate a dual functionality that links an inorganic substrate via an −O−Si− group and an organic polymer via an organic functional group −R.[29] Layers of organosilane are formed in a sequence as follows: (i) hydrolysis of alkoxysilanes to silanols ($R_nSi(OH)_{4-n}$), (ii) deposition of films via different methods, and (iii) curing of the films at an elevated temperature to ensure condensation to siloxanes and polysiloxanes ($(R-S-O-Si)_n$) and polymerization and to eliminate water.[30] The formed films act as a physical barrier restricting the penetration of corrosive species to the metal surface.[31,32]

A literature survey revealed that the protection behavior of a variety of silane sol−gel coatings such as tetraethoxysilane (TEOS),[33] trimethoxypropylsilane (TMPSi),[33] 3-glycidoxypropyl trimethoxysilane (GPTMS),[34] tris(2-methoxyethoxy)-vinylsilane (VTMOEO),[35] 3-aminopropyltriethoxysilane (APS),[36] (3-mercaptopropyl)triethoxysilane (MPTES),[37] tetraethylorthosilicate (TEOS),[38] 1,2-bis(triethoxysilyl)ethane (BTSE),[39,40] and bis[3-(triethoxysilyl)propyl]tetrasulfide (TESPT)[41] have been largely studied as attractive alternatives to the chromate. These coatings are a rapidly expanding technology resulting from their main advantages: good compatibility and high adhesion to a wide range of inorganic and organic interfaces, minimal environmental impact, and competitive pricing.[42,43] Furthermore, another important feature of these coatings is the barrier performance against electrolyte diffusion to the substrate, which is based on forming a dense layer with a three-dimensional network of siloxane.[44−46] Several factors such as the curing time, aging, concentration, pH, and chemical structure of the silanes are the main parameters that influence the properties of the final coating.[47−49]

In this article, the corrosion resistance and durability of three silanes (i.e., TESPT, BTSE, and VTES) for carbon steel 1018 substrates in an extremely high-salinity environment (4.5 wt % NaCl) is investigated. Carbon steel alloy was selected for this study since it is the main material used in building seawater desalination plant structures, water storage, tanks, and pipelines despite its low corrosion resistance. Also, a comparative study on the corrosion resistance of the three silanes was carried out along with the surface film characterization of each silane. The artificial seawater in this study has a sodium chloride concentration of 4.5 wt %, whereas other salts with trace amounts are neglected.

2. EXPERIMENTAL SECTION

2.1. Raw Materials. 1,2-Bis(triethoxysilyl)ethane (BTSE), bis[3-(triethoxysilyl)propyl]tetrasulfide (TESPT), and vinyl trimethylsilane (VTMS) with a purity of 96, ≥90, and 97%, respectively, were bought from Sigma-Aldrich (USA). The received silanes were used directly without any pretreatments. Figure 1 displays the molecular structures of each silane used

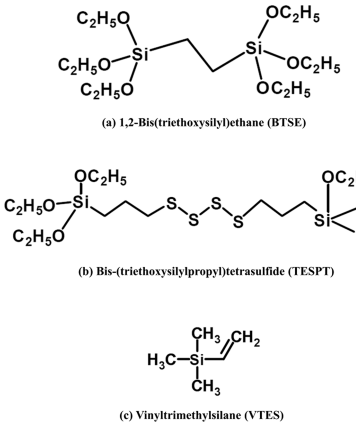

Figure 1. Molecular structures of different silanes.

in this study. The carbon steel 1018 bar with a diameter of 10 mm and length of 240 mm was bought from BDH Lab and Scientific Equipment Company (USA). The chemical composition of the carbon steel is mentioned in Table 1. The bar was cut into cylindrical pieces of 10 mm in thickness/height. Each piece was pre-fitted and sealed in a glass sleeve to cover the side of the cylindrical sample, exposing only the top and bottom. During corrosion testing, only the top surface was

Table 1. Chemical Composition (wt %) of Carbon Steel (Grade 1018)

element	composition (wt %)
carbon (C)	0.15−0.20
silicon (Si)	0.17−0.37
manganese (Mn)	0.60−0.90
sulfur (S)	≤0.050
phosphorus (P)	≤0.040

https://doi.org/10.1021/acsomega.3c00013
ACS Omega 2023, 8, 12886−12898

exposed to the NaCl electrolyte where the exposed area was 0.785 cm^2, while the other side was used for electrical contact.

2.2. Silane Solution Preparation. Three silane solutions were prepared to be investigated in this study. BTSE solution was prepared by mixing 4% BTSE, 0.4% acetic acid, 6% deionized water, and 89.6% methanol by volume. Then, the mixture was stirred for 1 h.[50] The pH of the prepared BTSE solution was measured to be 4.2. The TESPT solution with a 5% concentration by volume was prepared by adding the silane to a mixture of ethanol and deionized water then stirring for 10 min. The ratio of TESPT/deionized water/ethanol was 5/5/90, respectively. The pH of the TESPT solution was measured to be 7.2.[51] VTMS solution was prepared following the same preparation procedure of TESPT solution. The ratio of VTMS/deionaized water/ethanol was 5/5/90, respectively. The pH of the VTMS solution was measured to be 8.9. The TESPT and VTMS solutions in this work were prepared at a concentration of 5% by volume. All prepared silane solutions were maintained at room temperature for at least 48 h before use in order to increase the number of hydrolyzed silane molecules.[51]

2.3. Surface Treatment. Before applying the silane coating, the carbon steel pieces were polished with silicon carbide grinding papers gradually up to 3000 grade finishes. The polished surfaces were degreased using ultrasonic bath containing acetone for 5 min followed by another 5 min of degreasing using methanol. After cleaning the steel surface, it was immersed in a 2.5% sodium hydroxide solution for 10 min in order to improve the surface wettability. After this step (i.e., alkaline degreasing), the substrate surface became a water-break-free surface, meaning that the surface became completely free of contaminants, which decreases the number of active areas available for reacting with silanol groups in silane solution.[40] Afterward, the pretreated surface was rinsed with deionized water and dried with a hot air stream. Once the substrate surface pretreatment is finished, the steel surface becomes ready to be dipped into the prepared silane solutions. Based on the literature, all data presented in this study were obtained at a dipping time of 25 min.[52,53] Then, the effect of the curing time was tested to obtain the optimum curing time to be applied in this study. Potentiodynamic polarization tests were carried out in 4.5 wt % NaCl solution for silane-coated samples that were heated up to 120 °C for different time periods (10, 60, and 100 min) to evaluate the effect of the curing time on coating performance. The changes in the obtained corrosion current density (j_{corr}) with respect to the variation in the curing time are presented in Figure 2. Results showed that the j_{corr} for silane-treated samples remains the same (~0.058 $\mu A/cm^2$) throughout all tested times, which means that the protective performance of silane-treated samples against corrosion is independent of the curing time. Since there is no effect for the curing time, 60 min was considered a moderate time, and it was chosen in this study to be applied to all studied cases. The same coating procedure was followed for the formation of BTSE, TESPT, and VTMS coatings.

2.4. Corrosion Testing. An Autolab PGSTAT302N was used to apply potentiodynamic polarization (PDP), and electrochemical impedance spectroscopy (EIS) techniques were applied to evaluate the corrosion resistance performance of each silane coating in 4.5 wt % sodium chloride solution before and after the coating process on carbon steel substrates. Nova 2.0 software was utilized to control, monitor, and provide

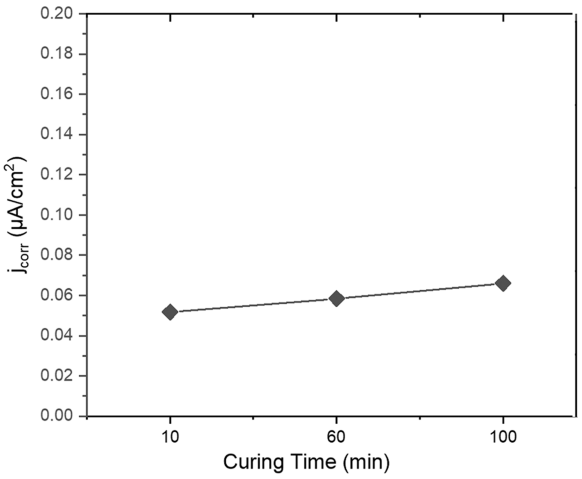

Figure 2. Change of the corrosion rate (j_{corr}) of TESPT-coated carbon steel samples immersed in 4.5 wt % NaCl solution at different curing times.

the experimental data as well as the resultant plots. The electrochemical testing was performed with a three-electrode electrochemical cell, which is composed of the freshly prepared carbon steel samples as the working electrode, a saturated Ag/AgCl reference electrode, and the counter electrode (platinum foil, 1 cm^2). In order to check the reliability and reproducibility of the resultant data, all experiments were repeated two to three times under the same conditions. Before starting any electrochemical measurements, the open-circuit potential (E_{OCP}) was tracked to reach a stable status to ensure the stability of the working electrode. The required test temperature was maintained using a constant temperature water bath.

After pre-immersing the silane-coated samples in sodium chloride to obtain the open-circuit potential E_{OCP} value, the PDP curves were recorded at a scan rate of 1 mV/s. The electrode potential was scanned within a range from −0.4 to 1 V with respect to the E_{OCP} (ASTM standards G5-87). All EIS tests were performed over a range of frequencies varying from 100 kHz to 0.1 Hz with 10 readings per decade. The AC signal amplitude was 10 mV.

2.5. Silane Film Analysis. Several techniques were applied in this work to analyze the characteristics of the silane film formed on the carbon steel substrate, such as Fourier-transform infrared reflection−absorption (FTIR-RA), X-ray photoelectron spectroscopy (XPS), scanning electron microscopy (SEM), and energy-dispersive X-ray spectroscopy (EDX). All surface measurements were performed on the carbon steel samples immediately after the corrosion testing.

FTIR-RA measurements were recorded using Tensor 27 (Bruker, Ettingen Germany) equipped with an attenuated total reflection (ATR) system. OPUS computer software (Bruker Germany) was used to collect the IR absorption spectra. The scans of wavelengths between 600 and 1400 cm^{-1} were obtained with a spectrum resolution of 4 cm^{-1}, and the number of scans was 16.

XPS spectra were collected on a Thermo ESCALAB 250 Xi system equipped with a monochromatic Al Kα X-ray source (1486.6 eV) with a spot size of 850 μm. The spectra were taken using Thermo Avantage software version 5.956. The analysis was performed using parameters for a narrow scan as follows: pass energy of 20 eV, 50 ms dwell time, and 0.1 eV

https://doi.org/10.1021/acsomega.3c00013
ACS Omega 2023, 8, 12886−12898

step size. All binding energy values were determined with reference to the C 1s peak at 284.6 eV.

SEM and EDX were used to study the morphology and the chemical composition of the silane film. This data was collected using a JEOL JSM-7001F scanning electron microscope (SEM) (JEOL Ltd., Tokyo, Japan) equipped with an Oxford INCAx-act energy-dispersive spectrometer (EDS). The applied acceleration voltage was 10 kV.

3. RESULTS AND DISCUSSION

3.1. Electrochemical Investigation for Different Silane Solutions. *3.1.1. Potentiodynamic Polarization Test.*

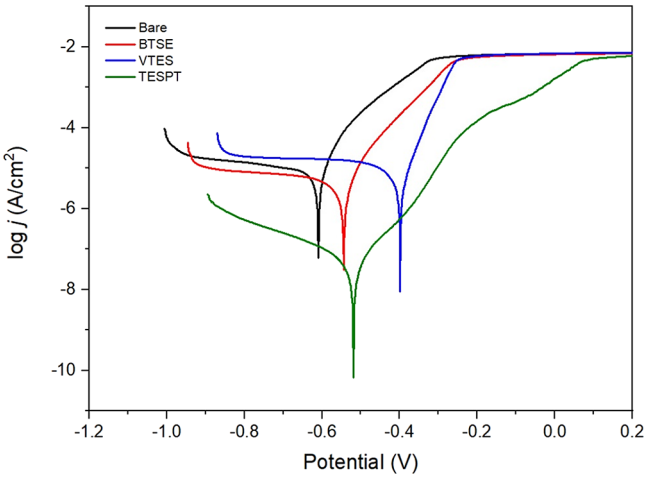

Figure 3. Potentiodynamic polarization curves of carbon steel in 4.5 wt % NaCl at 25 °C before and after coating the surface with different silane solutions vs Ag/AgCl.

Test. Figure 3 shows the potentiodynamic polarization curves for the corrosion behavior of uncoated and coated carbon steel with different silanes exposed to 4.5 wt % NaCl solution at 25 °C for 45 min. From the cathodic behavior of the polarization curves, it can be observed that both BTSE and TESPT coatings resulted in a decrease in the cathodic current densities. Regarding the VTES-coated carbon steel, no significant improvement in the cathodic current density value was observed, which is related to the high percentage of defects in the formed film. This result was proved also using the SEM test as will be discussed in Section 3.2.3. The decrease in the cathodic current density values is attributed to the coverage of the cathodic areas on the carbon steel surface by the silane film, which leads to a lower corrosion rate. This is an indication of the formation of a dense siloxane network at the coating–metal interface. The cathodic region of the polarization plot for each silane coating clearly shows that the TESPT has the lowest current density compared to others, thus showing 99.6% of a lower j than bare carbon steel.

The anodic current densities for all silane-coated surfaces were decreased, and the TESPT-coated carbon steel also showed the most significant reduction of j. Moreover, from the anodic scan of the VTES coating, a rapid increase in the anodic current density as the applied potential increases can be observed, and this is due to the quick dissolution rate. On the other hand, the sample coated with TESPT shows a considerably slow increase in the anodic current density as the applied potential increases. From the polarization plot, the VTES coating is inadequate in protecting the carbon steel from corrosion, while the TESPT coating provides the best corrosion protection. The protection efficiency of the TESPT results from the fully cross-linked silane film formed on the carbon steel surface. The characterization of the formed silane films will be explained in detail in the following sections using surface analysis techniques. Upon the completion of the polarization test, the carbon steel surfaces coated with VTES were damaged when they were inspected visually, while samples coated with TESPT were intact, which indicates that the quality of the protection of the TESPT coating is better than that of VTES.

The electrochemical polarization parameters are listed in Table 2: corrosion potential (E_{corr}), corrosion current density (j_{corr}), cathodic and anodic Tafel slopes (β_c and β_a), corrosion rate, and protection efficiency (η_P). The corrosion current density (j_{corr}) was obtained from the extrapolation of Tafel lines. However, all these electrochemical polarization parameters were determined using Nova software. From Table 2, it can be noticed that the E_{corr} of all carbon steel samples coated with BTSE, VTES, and TESPT shifted toward a positive direction by 70, 220, and 90 mV, respectively, versus Ag/AgCl. Although the E_{corr} value has been considerably improved after the application of the VTES coating, the corrosion rate was higher than in other samples due to the higher j_{corr} value as compared with BTSE and TESPT. The high corrosion current value means that, once the system exceeds the corrosion potential value (E_{corr}), the carbon steel surface will start to corrode rapidly.

The protection efficiencies for coated carbon steel samples were calculated using the equation below and are tabulated in Table 2:[54]

$$\eta_P\ (\%) = \left[\frac{(j_{corr}(\text{bare}) - j_{corr}(\text{coated})}{j_{corr}(\text{bare})}\right] \times 100 \quad (1)$$

As per Table 2, the coatings with regard to their corrosion resistance efficiencies in a descending order are TESPT, BTSE, and VTES. Also, a decreasing trend in the corrosion rate can be observed with the bare surface having the highest value and the surface with the TESPT coating having the lowest value. All data obtained from the potentiodynamic polarization data show the great potential of the TESPT coating in protecting

Table 2. Electrochemical Data Calculated Using the Potentiodynamic Polarization Method for Carbon Steel in 4.5 wt % NaCl at 25 °C Before and After the Formation of Different Silane Solutions versus Ag/AgCl

silane solution	j_{corr} (μA/cm^2)	E_{corr} (V)	β_c (mV/decade)	β_a (mV/decade)	corrosion rate (mm/year)	η_P (%)
bare	13.6	−0.61	190	85	0.315	
BTSE	5.3	−0.54	130	110	0.124	60.6
VTES	10.9	−0.39	210	80	0.253	19.9
TESPT	5.8×10^{-2}	−0.52	197	112	0.136×10^{-2}	99.6

https://doi.org/10.1021/acsomega.3c00013
ACS Omega 2023, 8, 12886−12898

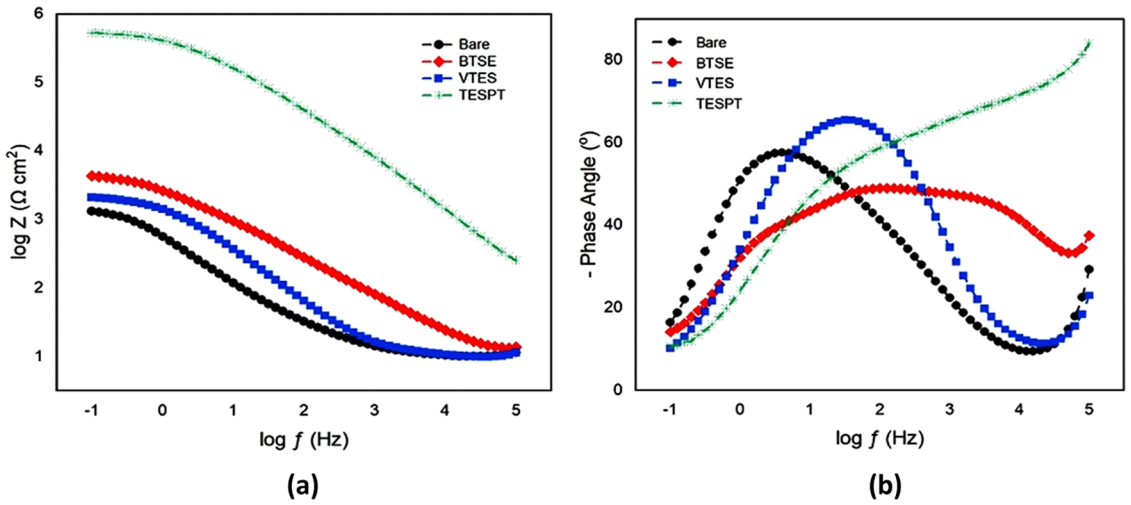

Figure 4. Bode plots of carbon steel in 4.5 wt % NaCl at 25 °C before and after coating the surface with different silane solutions: (a) log f vs log Z and (b) log f vs phase angle.

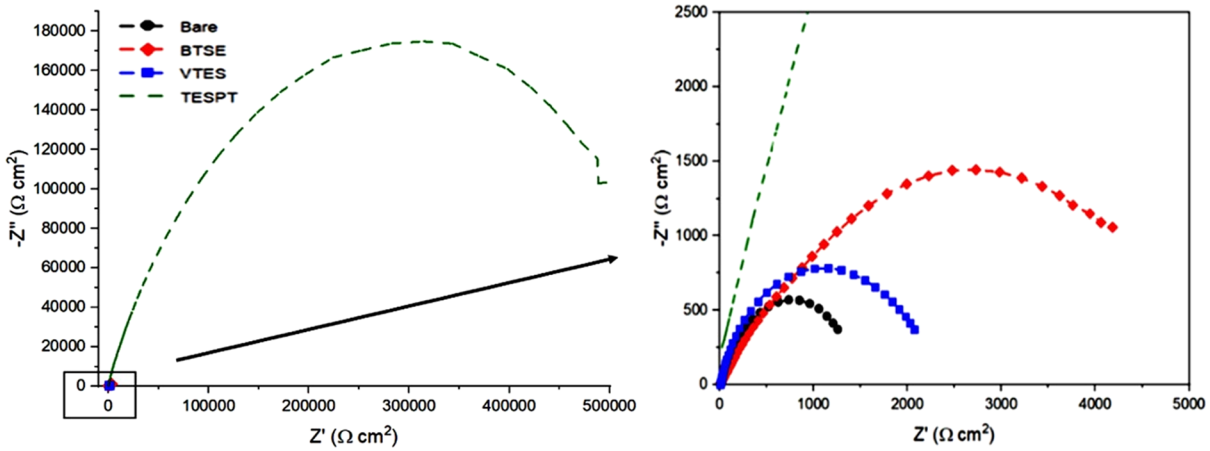

Figure 5. Nyquist plots of carbon steel in 4.5 wt % NaCl at 25 °C before and after coating the surface with different silane solutions. (The right graph shows the enlargement near the origin.)

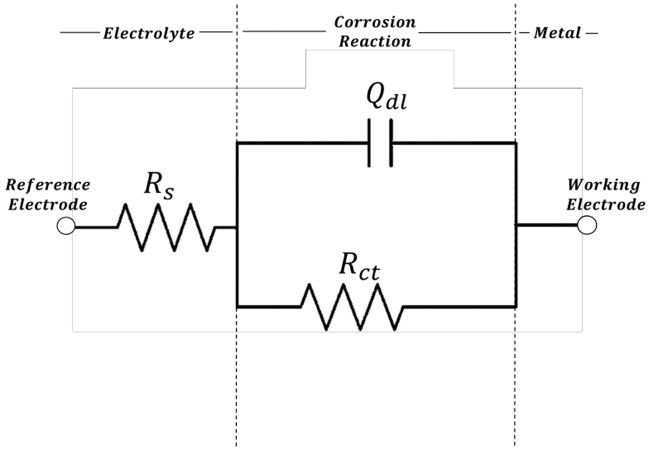

Figure 6. Equivalent electrical circuit model used for EIS data fitting for bare carbon steel.

carbon steel from corrosion during exposure to an aggressive chloride environment.

3.1.2. Electrochemical Impedance Spectroscopy (EIS). EIS was performed on uncoated and coated carbon steel with different silane films during the exposure to 4.5 wt % NaCl solution to examine the corrosion protection efficiency of each silane. Figures 4 and 5 show Bode and Nyquist plots for the corrosion behavior of uncoated and coated carbon steel with different silane films exposed to 4.5 wt % NaCl solution at 25 °C, respectively. For Bode plots, it has been known that the impedance at low frequencies is related to the corrosion resistance of samples, that is, the higher the impedance, the better the corrosion resistance of that system.[41,55] As expected from the polarization plot in Figure 3, the samples coated with BTSE and VTES silanes show a small improvement in the impedance values compared with the bare sample. On the other hand, carbon steel samples coated with TESPT solution show higher impedance values than the other silanes for the entire frequency region. Moreover, the Nyquist plot (Figure 5) shows that the samples coated with TESPT solution reveal the highest corrosion resistance to our corrosive medium (489 kΩ cm^2) compared with the uncoated one (1 kΩ cm^2), BTSE coating (4 kΩ cm^2), and VTES coating (2 kΩ cm^2).

As seen in Figure 4b, the bare carbon steel and the VTES-coated sample have one time constant at low frequencies (approximately below 10^2 Hz), which may refer to the formation of an oxide layer.[56] In the case of samples coated with TESPT and BTSE, a time constant showed up in the

https://doi.org/10.1021/acsomega.3c00013
ACS Omega 2023, 8, 12886−12898

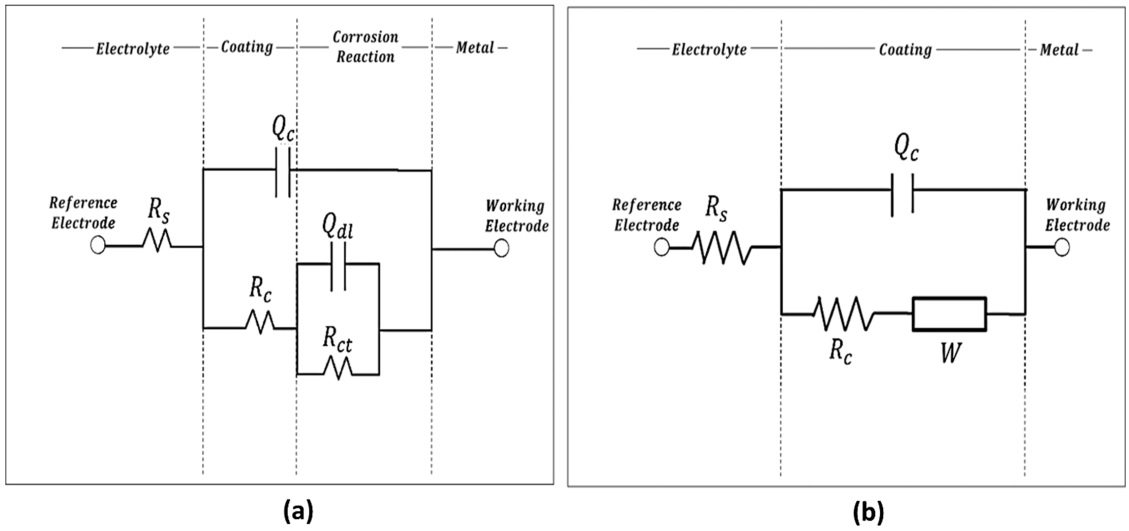

Figure 7. Equivalent electrical circuit models used for EIS data fitting for coated carbon steel with (a) TESPT and BTSE and (b) VTES.

Table 3. Impedance Parameters for Uncoated and Coated Carbon Steel with Different Silane Solutions in 4.5 wt % NaCl at 25 °C

		silane coating			oxide film			
		Q_c			Q_{dl}			
silane solution	R_s (Ω cm^2)	R_c (kΩ cm^2)	Y_{oc} (μF/cm^2)	n_c	R_{ct} (kΩ cm^2)	Y_{odl} (μF/cm^2)	n_{dl}	W (μF/cm^2)
bare	8.10				1.34	625.34	0.77	
TESPT	0.88	8.73	1.38	0.65	73.65	0.45	0.76	
BTSE	4.70	3.63	115.26	0.69	1.95	101.15	0.89	
VTES	6.67	1.70	424.61	0.79				9.47×10^{-3}

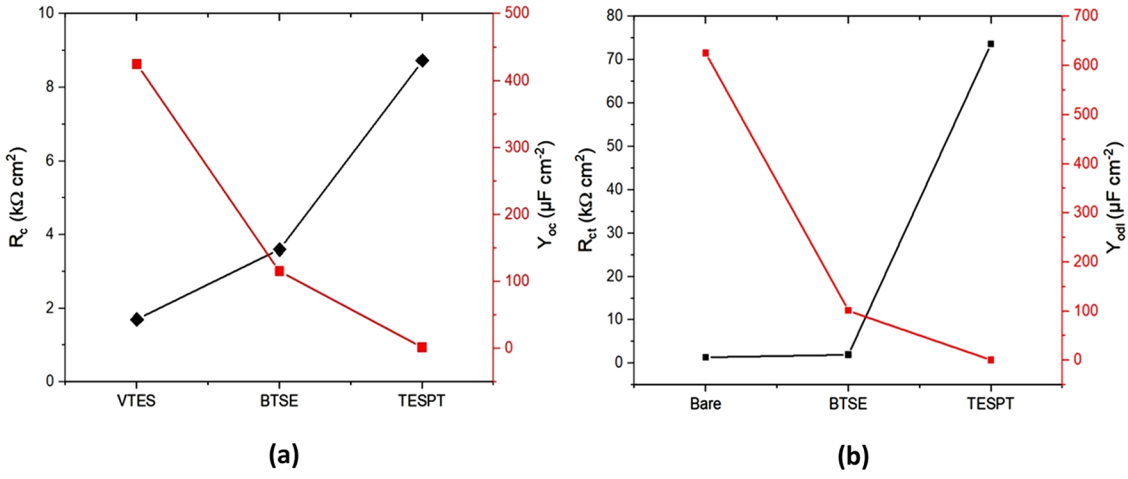

Figure 8. Change of resistances and CPE parameters of coated carbon steel samples with different silane solutions immersed in 4.5 wt % NaCl solution: (a) for VTES, BTSE, and TESPT and (b) for bare, BTSE, and TESPT.

high-frequency region (around 10^5 Hz) in the phase angle plot. This time constant can be attributed to the silane film.[56,57] The absence of the time constant at the high-frequency region in the phase angle plot of the VTES-coated sample may refer to the poor protective nature of the formed silane film.

Different equivalent electrical circuit (EEC) models have been applied to find the best fitted one for each studied case. Initially, the suggested EEC models were extracted from the number of time constants in the phase angle plot of each case. The best EEC models, which were utilized in fitting the impedance data of the studied cases, are illustrated in Figures 6 and 7. Two plots are displayed as examples to show the good agreement between the fitted and experimental data (Figures S1 and S2). Figure S1 shows the agreement between the fitted and recorded data for bare carbon steel sample in 4.5 wt % NaCl using the EEC model shown in Figure 6. Also, Figure S2 shows the agreement between the fitted and recorded data for BTSE-carbon steel samples using the EEC models illustrated in Figure 7. Values of these electrochemical parameters were calculated by fitting the EIS experimental data to the EEC model using Nova software. Constant-phase element (CPE) components are used in these circuits instead of the capacitive

https://doi.org/10.1021/acsomega.3c00013
ACS Omega 2023, 8, 12886−12898

Table 4. XPS Surface Composition (%) of VTES and TESPT-Coated Carbon Steel Before and After the Corrosion Testing

	VTES		TESPT	
element	before corrosion	after corrosion	before corrosion	after corrosion
C	22.04	18.59	55.38	54.68
O	58.84	54.04	22.51	24.74
Si	2.94	1.10	11.73	8.66
S			10.38	10.58
Fe	16.18	18.08		0.87
Cu		0.81		0.46
Cl		7.38		

elements in order to reduce the errors caused by surface roughness and the non-ideal deposition process of coating layers. The CPE components in these EEC models are named Q and defined by the CPE parameters (Y^0 and n). The EIS parameters obtained for the studied cases using EEC models are tabulated in Table 3.

Figure 6 illustrates the EEC model selected for the bare carbon steel immersed in 4.5 wt % NaCl at 25 °C. This EEC model includes one time constant and consists of the reference electrode, working electrode (i.e., carbon steel electrode), electrolyte resistance R_s, charge transfer resistance R_{ct}, and CPE of the double layer Q_{dl}, where R_{ct} and Q_{dl} parameters indicate the formation of an oxide layer after the exposure to the sodium chloride medium.

Regarding the coated samples with silane solutions, different EEC models were applied according to the time constants of each silane to give the best fitting results. Figure 7a illustrates the EEC model used for carbon steel coated with TESPT and BTSE that has two time constants and consists of the electrolyte resistance R_s, coating resistance R_c, and CPE of the silane coating Q_c, where the R_c and Q_c parameters are associated with the presence of a dense silane coating. The presence of the parameters (R_{ct} and Q_{dl}) indicates the formation of an oxide layer, indicating that water and chloride ions penetrate into the film and reach the metal surface, resulting in metal dissolution.[58] Nevertheless, from Table 3, which will be discussed below, it will be observed that the R_{ct} value of the TESPT-treated sample is much higher than that for the BTSE-treated sample, as shown in Figure 8b. This means that the formed BTSE layer was less dense and more porous, while the TESPT film was less porous due to the strong cross-linking of siloxane molecules. For the VTES-coated carbon steel immersed in 4.5 wt % NaCl solution, the designated EEC model consists of one time constant and includes the solution resistance R_s, coating resistance R_c, CPE of the silane coating Q_c, and Warburg impedance W (Figure 7b). The presence of the Warburg element is an indication that the diffusion rate was affecting the system where the electrolyte (water and ions) penetration through the coating film was the reason behind the diffusion in the EIS response due to the saturation of that film with the electrolyte. This means that the VTES film was very porous and could be easily penetrated by the corrosive ions.[58,59]

The change of the R_c and Q_c values of the coated carbon steel samples with different silane solutions is illustrated in Figure 8a. The strength of the cross-linking at the coating–metal interface can be estimated by the change in the R_c value because, as the silane film becomes denser, a high number of

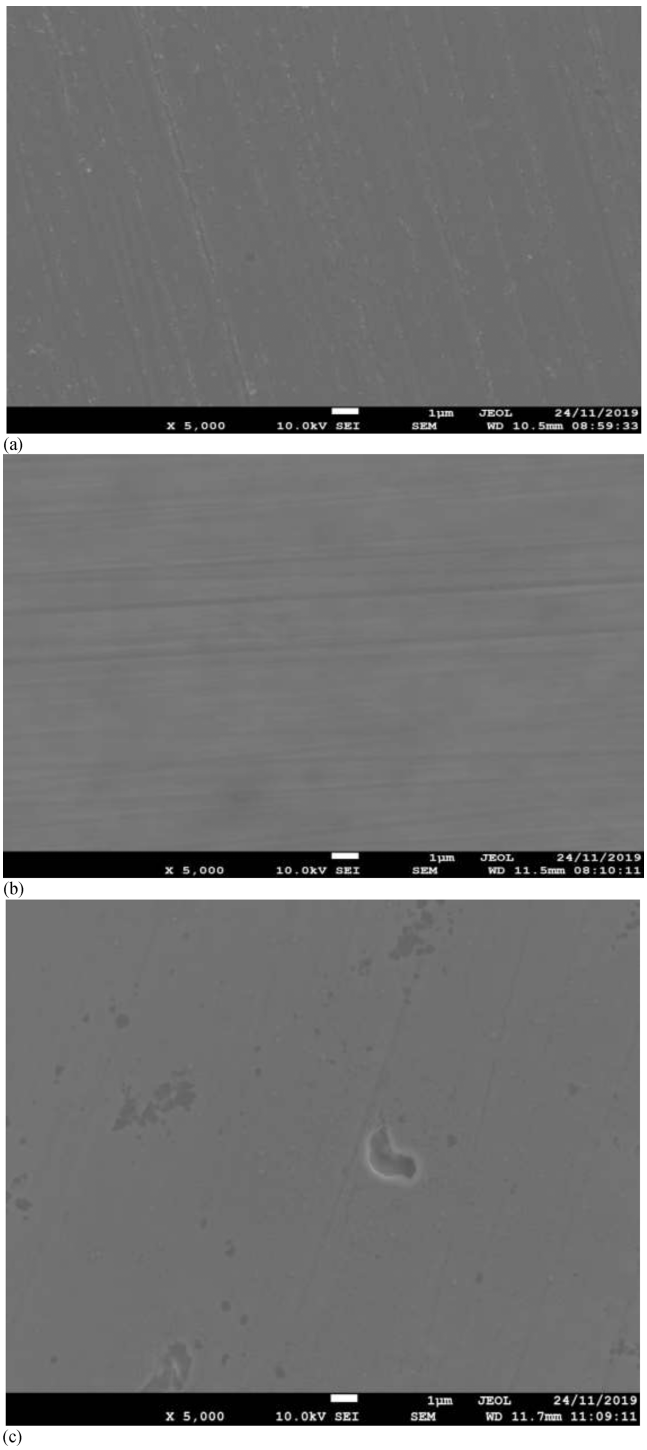

Figure 9. SEM micrographs of a carbon steel surface: (a) bare sample, (b) TESPT-coated sample, and (c) VTES-coated sample before the corrosion testing.

Table 5. Surface Composition (wt %) of Coated Carbon Steel with TESPT and VTES Silanes

element	TESPT	VTES
Fe	42.8	90.2
C	14.5	4.0
O	15.5	3.8
Si	11.4	2.0
S	15.7	

https://doi.org/10.1021/acsomega.3c00013
ACS Omega 2023, 8, 12886−12898

Table 6. Surface Composition (Wt %) of TESPT-Coated and Uncoated Carbon Steel before and after the Exposure to 4.5 Wt.% NaCl at 25 °C

	bare		TESPT	
element	before corrosion	after corrosion	before corrosion	after corrosion
Fe	99.3	98.0	42.8	51.7
Mn	0.4			
Cr	0.1			
O		0.9	15.5	14.6
S			15.7	13.7
C			14.5	12.1
Si	0.3		11.4	7.9
Na		0.8		
Cl		0.3		

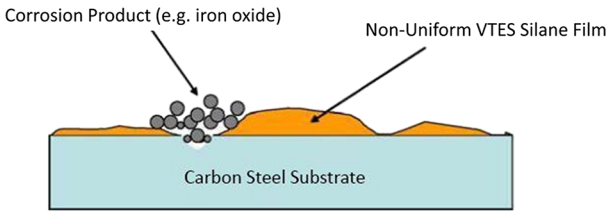

Figure 10. Poorly coated carbon steel substrate with a VTES silane film.

pores in that film is blocked and a high amount of water is evaporated, resulting in a decrease in the total pore area A_p, and thus the coating resistance increases. At the same time, the evaporation of water causes a decrease in the coating capacitance value Q_c.[51] Regarding the two electrochemical parameters related to the coating−metal interface (i.e., R_{ct} and C_{dl}), they are considered as an indication of the delamination of the formed coating and the initiation of the corrosion process. Consequently, the silane film that provides better protective performance against corrosion should result in a higher R_c, lower C_c, and higher W (if present) compared with the less efficient coating.[60] From Table 3, it can be observed that the coating resistance R_c value for carbon steel coated with the TESPT solution is much higher than that for the coated samples with BTSE and VTES solutions. The high value of R_c is associated with the formation of a denser and more uniform film formed by the TESPT solution, compared with the other two studied solutions. On the other hand, the coating capacitance for the three silanes is ascending in the following order TESPT, BTSE, and VTES. The decrease in the coating capacitance value supports the conclusion that the TESPT film is denser and more cross-linked than the other two silanes. This is because the formation of a stronger siloxane network reduces the amount of water absorbed through the film, and thus the C_c value decreases.[61] This is in case the coating thickness d of the three layers was assumed to be almost the same. Another reasonable justification for the decrease in the capacitance C_c is that the thickness of the TESPT layer formed on the carbon steel was larger than that of BTSE and VTES where the capacitance decreases as the coating thickness increases.

Based on the above results, it can be concluded that the TESPT silane film provides excellent and promising corrosion resistance for the carbon steel surface in 4.5 wt % NaCl solution compared to the VTES film, which showed poor corrosion protection performance. The corrosion resistance efficiency can be related to the pH of the silane solution and the isoelectric point (IEP) of the substrate surface, which is equal to the pH of the surface where the net charge is zero. It has been reported that, when the pH of the silane is higher than the pH of the IEP, the surface gains negative charges and vice versa.[62] In this study, the VTES film was prepared from a solution of pH ≈ 9, and since the isoelectric point (IEP) of the iron surface (∼8) is below 9,[63] the surface becomes charged negatively when immersed in the silane solution. As the iron surface is negative, the positive species of the silane solution will be absorbed by the surface. This results in an increase in the acidic character of the surface coated with the VTES solution. Since the steel surface becomes negatively charged, a number of $CH_2 = CH - SiO^-$ molecules will not completely react with the oxide layer during the condensation process. The presence of the unreacted VTES molecules at the coating−metal interface contributes to forming a low cross-linked structure and enhances the rate of water uptake into the film, thus reducing coating barrier properties. In addition, the acidic character causes a strong attraction of chloride ions toward the surface, hence the silane film resulting in defects in the coating film as well as accelerating substrate corrosion reactions.[64] Conversely, the TESPT film is prepared from a neutral solution (pH ≈ 7), and since the isoelectric point (IEP) of the iron surface (∼8) is greater than 7,[63] the surface becomes charged positively when immersed in the TESPT solution. In this way, the negative species of the silane solution are attracted to the positively charged surface and more covalent bonds are created between the silane film and the charged surface. In addition, this interaction results in an increase in the basic character of the coated surface. Thus, in the case of the formed TESPT film, there is no attraction force that promotes the penetration of chloride ions Cl^- into the film, which considers an indication of the high hydrophobicity of the TESPT.[31,52,64]

From electrochemical measurements illustrated in this section, it was concluded that, among the studied silanes in this work, the TESPT film exhibits the best corrosion protection performance while the VTES film performs the worst corrosion protection on carbon steel. For further verification, XPS, EDX, and SEM tests were conducted in this study to compare these two silanes (TESPT and VTES) only.

3.2. Surface Analysis of the Coated Carbon Steel.

3.2.1. X-ray Photoelectron Spectroscopy (XPS). To support the concept mentioned above, both TESPT and VTES films were examined using the X-ray photoelectron spectroscopy (XPS) technique before and after the exposure to the corrosive environment at 25 °C. By using this technique, we can identify the different elements present on the surface (and near-surface) of each film as well as the elemental changes that occurred after the exposure to NaCl solution. The XPS results of carbon steel surfaces coated with VTES and TESPT films are tabulated in Table 4. The XPS analysis performed on the TESPT-coated samples before being corroded did not show any iron or copper peak, meaning that a homogeneous silane film has covered the whole surface of the carbon steel substrate. In the case of the VTES film, the Fe peak was detected on the film surface before the exposure, meaning that the formed VTES film was not uniform and/or not completely covering the surface[55] as seen also in the SEM micrograph (Figure 9).

https://doi.org/10.1021/acsomega.3c00013
ACS Omega 2023, 8, 12886−12898

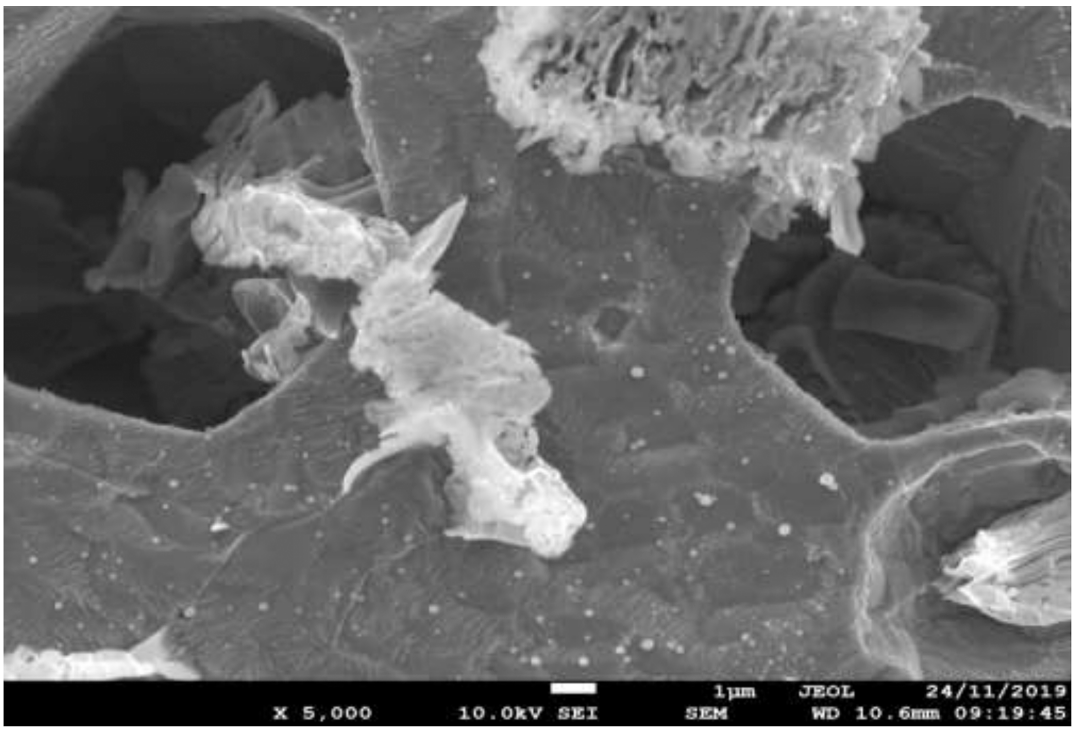

(a)

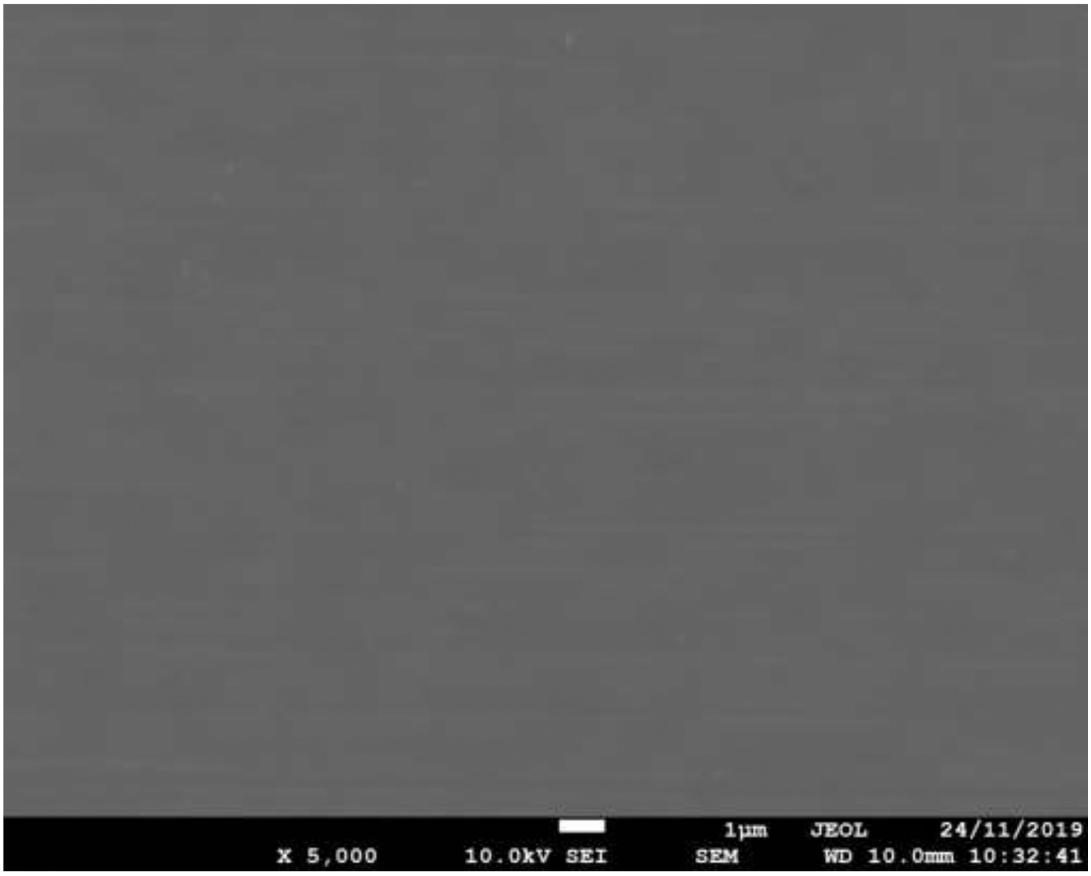

(b)

Figure 11. SEM micrographs of carbon steel surface: (a) bare sample after the exposure to 4.5 wt % NaCl solution at 25 °C and (b) TESPT-coated sample after the exposure to 4.5 wt % NaCl solution at 25 °C.

The silicon peak (Si 2p) at binding energies of 101.8 eV, shown in Figure S3, was obtained on the carbon steel surface coated with the TESPT film, which refers to the presence of Si − O bonds.[53] A minor reduction was observed in the atomic

https://doi.org/10.1021/acsomega.3c00013
ACS Omega 2023, 8, 12886−12898

percentage of silicon in the TESPT film before and after exposure, that is, 11.73% and 8.66%, respectively. Also, it can be observed from Table 4 that the TESPT film was able to retain most of its sulfur content after the application of the corrosion test. The results indicate that TESPT films on carbon steel surfaces remain stable even after being exposed to extremely high-chloride environments. The Si − O bonding suggests strong cross-linking at the film−metal interface. It is worth mentioning that the absence of the silane peak (Si 2p) at a binding energy of ∼103 eV, which is related to the presence of Si − OH bonds, means that no unhydrolyzed molecules were found in the formed TESPT film on the carbon steel surface as expected.[53,55]

However, the same silicon peak was present in the XPS data of the VTES-coated surface but with a low atomic percentage compared to that of TESPT. The silicon concentrations of the VTES and TESPT films were 2.94% and 11.73%, respectively, as listed in Table 4. The lower value suggests that the VTES film is not well cross-linked at the interface due to the presence of a number of unreacted molecules with OH groups of the substrate surface. As seen in Figure S4, the oxygen (O 1s) peak at a binding energy of 532 eV, which refers to the presence of O − Si bonds, was obtained for both tested films. In the case of the VTES film, another oxygen peak with a lower binding energy (530 eV) was observed, indicating the presence of oxygen as iron oxides (O − Fe).[50] This is an indication that the carbon steel substrate was poorly covered by the VTES film as the surrounding oxygen was not perfectly isolated from the alloy surface, which could be attributed to the presence of unreacted VTES molecules at the interface, resulting in a poorly cross-linked and high-porosity structure. In the case of the surface coated with TESPT solution, the oxygen peak at 530 eV was observed only after the exposure to sodium chloride solution (the substrate was fully covered with a dense layer of silane), as seen in Figure S5, with a low atomic percentage of this bond (1.97%).

The XPS analysis performed on VTES and TESPT films, before being corroded, showed carbon peaks at different binding energies, as seen in Figure S6. The carbon peak at 284.6 eV refers to the formation of C − H bonds, while the peak at ∼286 eV corresponds to the formation of C − O bonds.[53] These two carbon peaks were also observed on the substrate surfaces coated with VTES and TESPT solutions. Another carbon peak at 288.3 eV was detected only on the surface coated with the VTES film, suggesting the formation of C = O bonds. The existence of the C = O bonds may refer to the degradation of the outer layers of the VTES film resulting from the oxidation of some carbon molecules contained in the silane film. All these observations indicate that the substrate was poorly covered by the VTES film. From Table 4, the XPS spectra of the TESPT film did not include any chlorine or sodium peaks after the exposure to sodium chloride solution. In the VTES film, on the contrary, a detectable amount of chloride ion was found after immersion in 4.5 wt % NaCl. The data obtained from the XPS strongly supports our preceding results on TESPT, which are further verified by the EDX results discussed in the following section.

3.2.2. Energy-Dispersive X-ray Spectroscopy (EDX). The energy-dispersive X-ray spectroscopy (EDX) technique was performed on the coated carbon steel samples with VTES and TESPT solutions in order to support the results obtained from XPS tests and electrochemical measurements. The EDX spectra of the carbon steel surfaces coated with TESPT and VTES silanes are shown in Figure S7, and the data are listed in Table 5. The results showed that the percentage of iron on the TESPT-coated surface was significantly less than that of the surface coated with the VTES film. This is due to the nature of the VTES film (less dense, porous, poor surface coverage, etc.).

Furthermore, EDX results showed that the TESPT film has a silicon content of 11.4%, while the VTES film has a silicon content of 2%. The low silicon content, again, is an indication of the formation of a non-uniform VTES film on the carbon steel surface. This may result from the poorly defined cross-linking of the silane with the substrate due to the deficiency of the $CH_2 = CH - SiO^-$ molecules in the VTES film to react with an iron oxide film.

The EDX test was also performed for TESPT-coated and uncoated carbon steel before and after the exposure to 4.5 wt % NaCl solution at 25 °C. The EDX spectra of the bare carbon steel surface before and after the immersion in sodium chloride solution are shown in Figure S8, while the EDX spectra of the TESPT-coated carbon steel surface before and after the corrosion testing are shown in Figure S9. EDX results confirmed the results obtained from the XPS data presented earlier, which are listed in Table 6. In the case of the uncoated surface, the results showed that the amount of iron was maintained before and after the corrosion testing and, since bare carbon steel alloys normally contain manganese and silicon elements (as mentioned in Table 1), small peaks of these elements were also observed. As expected, the percentage of iron on the coated surface was lower than the bare sample, which implies that the carbon steel was well covered by a uniform TESPT film. By comparing the iron content in the TESPT film before and after corrosion testing, a slight increase in the iron content is observed where it increased from 42.8 to 51.7 wt % after the exposure to NaCl solution. Moreover, the EDX results show that the silicon and sulfur amounts in the TESPT film decreased after the exposure to NaCl solution from 11.4 to 7.9 wt % and from 15.7 to 13.7 wt %, respectively. These slight changes in iron, sulfur, and silicon contents after the corrosion testing are an indication of the stability of the TESPT film on the carbon steel surface. A further observation is that the percentage of chloride ions (Cl^-) in the uncoated carbon steel surface was approximately 0.3% after the corrosion testing, while no chlorine peaks were detected in the TESPT film even after the exposure to the corrosive sodium chloride solution. This confirms that the TESPT film does not promote the penetration of chloride ions due to its hydrophobic structure, indicating that this film provides sufficient protection for the carbon steel substrates in NaCl solution.

3.2.3. Scanning Electron Microscopy (SEM). The SEM examinations were important to understand the surface features of the formed films from a microstructure point of view. Figure 9a shows the SEM scan of a freshly polished carbon steel sample before coating application. Figure 9b,c shows the SEM images of the polished carbon steel samples after the formation of TESPT and VTES films, respectively. A significant difference in the surface homogeneity can be distinctly observed where the TESPT film was more compact and uniform compared with the VTES film. The micrograph of the surface coated with TESPT silane solution in Figure 9b shows that the substrate is totally covered with an intact TESPT coating, while Figure 9c shows that there are some defective sites that are poorly covered by the VTES coating, as shown schematically in Figure 10. The presence of these defective areas on the surface promotes corrosion initiation as

https://doi.org/10.1021/acsomega.3c00013
ACS Omega 2023, 8, 12886−12898

a result of the penetration of the corrosive ions. The data obtained from both the SEM and EDX tests confirm the formation of a homogeneous TESPT film on the surface of the carbon steel. While in the case of the VTES silane, the EDX and SEM techniques illustrate the reason behind the failure of the VTES-coating in protecting the carbon steel substrate against corrosion as also indicated by the electrochemical methods. The reason behind this failure is the insufficient cross-linking of the VTES with carbon steel due to the failure of some VTES molecules to react with the OH groups and create covalent bonds with the charged surface.

Figure 11 shows the surface of bare and TESPT-coated carbon steel substrate scanned after the exposure to the sodium chloride solution. The resulting scanning electron micrographs showed that the bare carbon steel surface was intensively destroyed after the exposure to the aggressive chloride solution at 25 °C for 45 min, and a formation of deep pits was observed in Figure 11a resulting from the aggressive chloride ions attack. For TESPT-coated surfaces, by comparing the SEM image in Figure 9b with the image in Figure 11a, both images are approximately the same and no pits, corrosion products, or cracks are detected on the surface of the carbon steel (the sample surface after performing the test was as shiny as the surface before the test). These results indicated that the TESPT film provided excellent corrosion protection performance to the carbon steel substrate due to its hydrophobic nature.

4. CONCLUSIONS

Overall, this work presents a facile and cost-effective method for mitigating carbon steel corrosion in marine environments. Among the three silanes (TESPT, BTSE, and VTES), the TESPT film (pH ≈ 7) has the best corrosion resistance performance on the carbon steel surface in the aggressive chloride environment, that is, 99.6%. The high corrosion resistance of the TESPT film is due to the hydrophobic nature of this silane, which leads to the formation of a stable, dense film. As verified by electrochemical measurements, the carbon steel samples treated with VTES solution of pH ≈ 9, which is higher than the isoelectric point (IEP) of the substrate surface, resulted in a low resistance against chloride ion ingress. These results were supported by XPS and SEM/EDX analysis.

■ ASSOCIATED CONTENT

Supporting Information

The Supporting Information is available free of charge at https://pubs.acs.org/doi/10.1021/acsomega.3c00013.

Agreement between the experimental and fitted data using EEC model, XPS spectra, and EDX spectra (PDF)

■ AUTHOR INFORMATION

Corresponding Author

Mohammad H. BinSabt − *Chemistry Department, Faculty of Science, Kuwait University, Safat 13060, Kuwait;* orcid.org/0000-0003-4057-233X; Phone: +965 24985587; Email: mohammad.binsabt@ku.edu.kw; Fax: +965 24816482

Authors

Fadhel A. Azeez − *Chemical Engineering Department, College of Engineering and Petroleum, Kuwait University, Safat 13060, Kuwait*

Nour Suleiman − *Chemical Engineering Department, College of Engineering and Petroleum, Kuwait University, Safat 13060, Kuwait*

Complete contact information is available at: https://pubs.acs.org/10.1021/acsomega.3c00013

Notes

The authors declare no competing financial interest.

■ ACKNOWLEDGMENTS

The instrumentation facilities through grant nos. GS01/01 and GS02/08, Science Analytical Facilities (Department of Chemistry), and RSPU instrumentation facilities are all highly appreciated.

■ REFERENCES

(1) Revie, R. W. *Corrosion and corrosion control: an introduction to corrosion science and engineering*; 4th ed.; John Wiley & Sons: Hoboken, NJ, USA, 2008.

(2) Speight, J. G. *Oil and gas corrosion prevention: From surface facilities to refineries*; Elsevier Science & Technology: Watham, MA, USA, 18 March 2014.

(3) Adumene, S.; Khan, F.; Adedigba, S.; Zendehboudi, S.; Shiri, H. Dynamic risk analysis of marine and offshore systems suffering microbial induced stochastic degradation. *Reliab. Eng. Syst. Saf.* **2021**, *207*, No. 107388.

(4) Khodabux, W.; Liao, C.; Brennan, F. Characterisation of pitting corrosion for inner section of offshore wind foundation using laser scanning. *Ocean Eng.* **2021**, *230*, No. 109079.

(5) Ahmad, Z., *Principles of corrosion engineering and corrosion control*; 1st ed.; Elsevier Ltd: Oxford, UK, 2006.

(6) El Basiony, N. M.; Tawfik, E. H.; El-raouf, M. A.; Fadda, A. A.; Waly, M. M. Synthesis, characterization, theoretical calculations (DFT and MC), and experimental of different substituted pyridine derivatives as corrosion mitigation for X-65 steel corrosion in 1M HCl. *J. Mol. Struct.* **2021**, *1231*, No. 129999.

(7) Loto, C. A.; Loto, R. T.; Popoola, P. A. Evaluation of cathodic protection of mild steel with magnesium anodes in 0.5 M HCL. *Chem. Data Collect.* **2019**, *22*, No. 100246.

(8) Paik, J. K.; Melchers, R. E., *Condition assessment of aged structures*; Elsevier, 2014.

(9) Wang, J.; Wang, N.; Liu, M.; Ge, C.; Hou, B.; Liu, G.; Sun, W.; Hu, Y.; Ning, Y. Hexagonal boron nitride/poly (vinyl butyral) composite coatings for corrosion protection of copper. *J. Mater. Sci. Technol.* **2022**, *96*, 103−112.

(10) Herrasti Gonzalez, P.; Ponce de Leon, C.; Walsh, F. C. The corrosion behaviour of nanograined metals and alloys. *Rev. Metal.* **2012**, *48*, 377−394.

(11) Poon, J.; Madden, D. C.; Welbourn, R. J. L.; Allen, F. J.; Khan, F.; Sonke, H.; Clarke, S. M. Corrosion inhibition of steel in seawater through surface phosphate formed from oil. *Surf. Coat. Technol.* **2021**, *410*, No. 126970.

(12) Piao, N.; Wang, L.; Anwar, T.; Feng, X.; Sheng, S.; Tian, G.; Wang, J.; Tang, Y.; He, X. Corrosion resistance mechanism of chromate conversion coated aluminium current collector in lithium-ion batteries. *Corros. Sci.* **2019**, *158*, No. 108100.

(13) Hu, Y.-t.; Zheng, L.; Yan, H.-j.; Wu, L.-k.; Lin, X.-j.; Cao, F.-h.; Jiang, M.-y. Improving hot corrosion resistance of aluminized TiAl alloy by anodization and pre-oxidation. *Trans. Nonferrous Met. Soc. China* **2021**, *31*, 193−206.

(14) Jiang, L.; Chen, Z. Q.; Lu, H. B.; Ke, H. B.; Yuan, Y.; Dong, Y. M.; Meng, X. K. Corrosion protection of NiNb metallic glass coatings for 316SS by magnetron sputtering. *J. Mater. Sci. Technol.* **2021**, *79*, 88−98.

(15) Cheng, L.; Lou, F.; Guo, W. Corrosion protection of the potassium silicate conversion coating. *Vacuum* **2020**, *176*, No. 109325.

(16) Huang, X.; Yu, L.; Dong, Y. Corrosion resistance of a novel ceria doped aluminum phosphate ceramic coating on cast Al-Si alloy by steam-assisted curing. *Corros. Sci.* **2021**, *182*, No. 109256.
(17) Susarla, S.; Chilkoor, G.; Kalimuthu, J. R.; Saadi, M. A. S. R.; Cui, Y.; Arif, T.; Tsafack, T.; Puthirath, A. B.; Sigdel, P.; Jasthi, B.; Sudeep, P. M.; Hu, L.; Hassan, A.; Castro-Pardo, S.; Barnes, M.; Roy, S.; Verduzco, R.; Kibria, M. G.; Filleter, T.; Lin, H.; Solares, S. D.; Koratkar, N.; Gadhamshetty, V.; Rahman, M. M.; Ajayan, P. M. Corrosion Resistance of Sulfur−Selenium Alloy Coatings. *Adv. Mater.* **2021**, *33*, 2104467.
(18) Wang, X.; Lin, Z. Robust, Hydrophobic Anti-corrosion Coating Prepared by PDMS Modified Epoxy Composite with Graphite Nanoplatelets/Nano-silica Hybrid Nanofillers. *Surf. Coat. Technol.* **2021**, No. 127440.
(19) Siddiqui, A. R.; Maurya, R.; Katiyar, P. K.; Balani, K. Superhydrophobic, self-cleaning carbon nanofiber CVD coating for corrosion protection of AISI 1020 steel and AZ31 magnesium alloys. *Surf. Coat. Technol.* **2020**, *404*, No. 126421.
(20) Zhang, H. D.; Chen, A. Y.; Gan, B.; Jiang, H.; Gu, L. J. Corrosion protection investigations of carbon dots and polydopamine composite coating on magnesium alloy. *J. Magnesium Alloys* **2022**, *10*, 1358−1367.
(21) Chen, Y.; Zhang, G.; Zhang, G.; Ma, C. Rapid curing and self-stratifying lacquer coating with antifouling and anticorrosive properties. *Chem. Eng. J.* **2021**, *421*, No. 129755.
(22) Peng, G.; Qiao, Q.; Huang, K.; Wu, J.; Wang, Y.; Fu, X.; Zhang, Z.; Fang, T.; Zhang, B.; Huang, Y.; Li, X. Ni-Fe-MoO42-LDHs/epoxy resin varnish: A composite coating on carbon steel for long-time and active corrosion protection. *Prog. Org. Coat.* **2020**, *140*, No. 105514.
(23) Liu, T.; Zhao, H.; Li, J.; Zhang, D.; Zheng, W.; Wang, L. POSS-tetraaniline based giant molecule: Synthesis, self-assembly, and active corrosion protection of epoxy-based organic coatings. *Corros. Sci.* **2020**, *168*, No. 108555.
(24) Yaseen, W. K.; Marpu, S. B.; Golden, T. D.; Omary, M. A. Synthesis and evaluation of a novel fluorinated poly (hexafluoroisopropyl methacrylate) polymer coating for corrosion protection on aluminum alloy. *Surf. Coat. Technol.* **2020**, *404*, No. 126444.
(25) Chen, X.; Wen, S. F.; Liu, Z. Q.; Yue, Z. F. Hybrid siloxane-epoxy coating reinforced by worm-like graphene oxide with improved mechanical properties and corrosion resistance. *Mater. Des.* **2021**, *207*, No. 109852.
(26) Suárez-Vega, A.; Agustín-Sáenz, C.; O'Dell, L. A.; Brusciotti, F.; Somers, A.; Forsyth, M. Properties of hybrid sol-gel coatings with the incorporation of lanthanum 4-hydroxy cinnamate as corrosion inhibitor on carbon steel with different surface finishes. *Appl. Surf. Sci.* **2021**, *561*, No. 149881.
(27) Zhang, S.-J.; Cao, D.-L.; Xu, L.-K.; Tang, J.-K.; Meng, R.-Q.; Li, H.-D. Corrosion resistance of a superhydrophobic dodecyltrimethoxysilane coating on magnesium hydroxide-pretreated magnesium alloy AZ31 by electrodeposition. *Colloids Surf., A* **2021**, *625*, No. 126914.
(28) Tavangar, R.; Naderi, R.; Mahdavian, M. Acidic surface treatment of mild steel with enhanced corrosion protection for silane coatings application: The effect of zinc cations. *Prog. Org. Coat.* **2021**, *158*, No. 106384.
(29) Kanoza, M.; Flis-Kabulska, I.; Flis, J. Effect of aging in air and immersion into phosphate solution on protectiveness and transformations of vinyltriethoxy silane nanofilms on iron. *Corros. Sci.* **2012**, *61*, 224−230.
(30) Flis, J.; Kanoza, M. Electrochemical and surface analytical study of vinyl-triethoxy silane films on iron after exposure to air. *Electrochim. Acta* **2006**, *51*, 2338−2345.
(31) Zhu, D.; van Ooij, W. J. Enhanced corrosion resistance of AA 2024-T3 and hot-dip galvanized steel using a mixture of bis-[triethoxysilylpropyl] tetrasulfide and bis-[trimethoxysilylpropyl] amine. *Electrochim. Acta* **2004**, *49*, 1113−1125.
(32) Franquet, A.; Terryn, H.; Vereecken, J. Study of the effect of different aluminium surface pretreatments on the deposition of thin non-functional silane coatings. *Surf. Interface Anal.* **2004**, *36*, 681−684.
(33) Javanpour, B.; Azadbeh, M.; Mozammel, M. Effect of Chemical Composition of Tetraethoxysilane and trimethoxy (Propyl) silane hybrid sol on hydrophobicity and corrosion resistance of anodized aluminum. *Silicon* **2020**, *12*, 867−882.
(34) Hernández-Barrios, C. A.; Saavedra, J. A.; Higuera, S. L.; Coy, A. E.; Viejo, F. Effect of cerium on the physicochemical and anticorrosive features of TEOS-GPTMS sol-gel coatings deposited on the AZ31 magnesium alloy. *Surf. Interfaces* **2020**, *21*, No. 100671.
(35) Zhu, H.; Qu, X.; Hu, Y.; Xie, H.; Chen, Z. Corrosion inhibition of flaky aluminium powders prepared through sol−gel process. *Corros. Sci.* **2011**, *53*, 481−486.
(36) Lashgari, S. M.; Yari, H.; Mahdavian, M.; Ramezanzadeh, B.; Bahlakeh, G.; Ramezanzadeh, M. Unique 2-methylimidazole based Inorganic Building Brick nano-particles (NPs) functionalized with 3-aminopropyltriethoxysilane with excellent controlled corrosion inhibitors delivery performance; Experimental coupled with molecular/DFT-D simulations. *J. Taiwan Inst. Chem. Eng.* **2020**, *117*, 209−222.
(37) Xavier, J. R. Electrochemical, mechanical and adhesive properties of surface modified NiO-epoxy nanocomposite coatings on mild steel. *Mater. Sci. Eng., B* **2020**, *260*, No. 114639.
(38) Alibakhshi, E.; Ghasemi, E.; Mahdavian, M.; Ramezanzadeh, B.; Farashi, S. Active corrosion protection of Mg-Al-PO_4^{3-} LDH nanoparticle in silane primer coated with epoxy on mild steel. *J. Taiwan Inst. Chem. Eng.* **2017**, *75*, 248−262.
(39) BinSabt, M. H.; Galal, A.; Al Kharafi, F. M.; Abditon, M. Improving corrosion protection of Al97Mg3 alloy in neutral sodium chloride solution by 1, 2-bis (triethoxysilyl) ethane coating. *Appl. Surf. Sci.* **2019**, *465*, 143−153.
(40) Al-Saadi, S.; Banerjee, P. C.; Raman, R. K. S. Corrosion of bare and silane-coated mild steel in chloride medium with and without sulphate reducing bacteria. *Prog. Org. Coat.* **2017**, *111*, 231−239.
(41) Zhu, H. Y.; Chen, Y.; Liu, Y. P.; Sun, W. W.; Chen, S. G. Analytical characterization and corrosion behavior of non-functional bis-silane pre-treated carbon steel substrates. *Adv. Mater. Res. (Switz.)* **2009**, *79*, 1091−1094.
(42) Ramasamy, S.; Tewari, S. N.; Lee, K. N.; Bhatt, R. T.; Fox, D. S. Mullite−gadolinium silicate environmental barrier coatings for melt infiltrated SiC/SiC composites. *Surf. Coat. Technol.* **2011**, *205*, 3578−3581.
(43) Trabelsi, W.; Triki, E.; Dhouibi, L.; Ferreira, M. G. S.; Zheludkevich, M. L.; Montemor, M. F. The use of pre-treatments based on doped silane solutions for improved corrosion resistance of galvanised steel substrates. *Surf. Coat. Technol.* **2006**, *200*, 4240−4250.
(44) Dias, S. A. S.; Lamaka, S. V.; Nogueira, C. A.; Diamantino, T. C.; Ferreira, M. G. S. Sol−gel coatings modified with zeolite fillers for active corrosion protection of AA2024. *Corros. Sci.* **2012**, *62*, 153−162.
(45) Montemor, M. F.; Ferreira, M. G. S. Electrochemical study of modified bis-[triethoxysilylpropyl] tetrasulfide silane films applied on the AZ31 Mg alloy. *Electrochim. Acta* **2007**, *52*, 7486−7495.
(46) Naderi, R.; Fedel, M.; Deflorian, F.; Poelman, M.; Olivier, M. Synergistic effect of clay nanoparticles and cerium component on the corrosion behavior of eco-friendly silane sol−gel layer applied on pure aluminum. *Surf. Coat. Technol.* **2013**, *224*, 93−100.
(47) Romano, A.-P.; Fedel, M.; Deflorian, F.; Olivier, M.-G. Silane sol−gel film as pretreatment for improvement of barrier properties and filiform corrosion resistance of 6016 aluminium alloy covered by cataphoretic coating. *Prog. Org. Coat.* **2011**, *72*, 695−702.
(48) Asadi, N.; Naderi, R.; Saremi, M.; Arman, S. Y.; Fedel, M.; Deflorian, F. Study of corrosion protection of mild steel by eco-friendly silane sol−gel coating. *J. Sol-Gel Sci. Technol.* **2014**, *70*, 329−338.
(49) Taheri, M.; Naderi, R.; Saremi, M.; Mahdavian, M. Development of an ecofriendly silane sol-gel coating with zinc acetylacetonate corrosion inhibitor for active protection of mild steel in sodium chloride solution. *J. Sol-Gel Sci. Technol.* **2017**, *81*, 154−166.

https://doi.org/10.1021/acsomega.3c00013
ACS Omega 2023, 8, 12886−12898

(50) Subramanian, V.; Van Ooij, W. J. Effect of the amine functional group on corrosion rate of iron coated with films of organofunctional silanes. *Corrosion* **1998**, *54*, 204−215.
(51) Van Ooij, W. J.; Zhu, D.; Stacy, M.; Seth, A.; Mugada, T.; Gandhi, J.; Puomi, P. Corrosion protection properties of organofunctional silanes—an overview. *Tsinghua Sci. Technol.* **2005**, *10*, 639−664.
(52) Al-Saadi, S. H. M. *Silane coatings for mitigation of microbiologically influenced corrosion of mild steel*; Monash University, 2013.
(53) Montemor, M. F.; Rosqvist, A.; Fagerholm, H.; Ferreira, M. G. S. The early corrosion behaviour of hot dip galvanised steel pretreated with bis-1, 2-(triethoxysilyl) ethane. *Prog. Org. Coat.* **2004**, *51*, 188−194.
(54) Popov, B. N., *Corrosion engineering: principles and solved problems*; Elsevier, 2015.
(55) Cabral, A. M.; Duarte, R. G.; Montemor, M. F.; Ferreira, M. G. S. A comparative study on the corrosion resistance of AA2024-T3 substrates pre-treated with different silane solutions: Composition of the films formed. *Prog. Org. Coat.* **2005**, *54*, 322−331.
(56) Calabrese, L.; Bonaccorsi, L.; Caprì, A.; Proverbio, E. Electrochemical behavior of hydrophobic silane−zeolite coatings for corrosion protection of aluminum substrate. *J. Coat. Technol. Res.* **2014**, *11*, 883−898.
(57) Zandi Zand, R.; Flexer, V.; De Keersmaecker, M.; Verbeken, K.; Adriaens, A. Self-healing silane coatings of cerium salt activated nanoparticles. *Mater. Corros.* **2016**, *67*, 693−701.
(58) Meng, F.; Liu, L. Electrochemical evaluation technologies of organic coatings. *Coat. Thin-Film Technol.* **2018**, *1*, 13.
(59) Gayosso, M. J. H.; Olivares, G. Z.; Ordaz, N. R.; Ramirez, C. J.; Esquivel, R. G.; Viveros, A. P. Microbial consortium influence upon steel corrosion rate, using polarisation resistance and electrochemical noise techniques. *Electrochim. Acta* **2004**, *49*, 4295−4301.
(60) Song, J.; Van Ooij, W. J. Bonding and corrosion protection mechanisms of γ-APS and BTSE silane films on aluminum substrates. *J. Adhes. Sci. Technol.* **2003**, *17*, 2191−2221.
(61) Calderón-Gutierrez, J. A.; Bedoya-Lora, F. E. Barrier property determination and lifetime prediction by electrochemical impedance spectroscopy of a high performance organic coating. *Dyna* **2014**, *81*, 97−106.
(62) Mittal, K. L. *Silanes and Other Coupling Agents*; *Vol. 4*. CRC Press, 2007.
(63) Nobbmann, U., *Nanomaterial Isoelectric Points IEPs*; Malvern Panalytical Ltd.: Malvern, UK 2017.
(64) Zand, B. N.; Mahdavian, M. Evaluation of the effect of vinyltrimethoxysilane on corrosion resistance and adhesion strength of epoxy coated AA1050. *Electrochim. Acta* **2007**, *52*, 6438−6442.

https://doi.org/10.1021/acsomega.3c00013
ACS Omega 2023, 8, 12886−12898